

# Form Factor Dark Matter

Brian Feldstein, A. Liam Fitzpatrick, Emanuel Katz

*Physics Department*

*Boston University, Boston, MA 02215, USA*

---

## Abstract

We present a dynamical alternative to inelastic dark matter as a way of reconciling the modulating signal seen at DAMA with null results at other direct detection experiments. The essential ingredient is a new form factor which introduces momentum dependence in the interaction of dark matter with nuclei. The role of the form factor is to suppress events at low momentum transfer. We find that a form factor approach is most likely not viable in the context of the standard halo model, however it is consistent with halo models suggested by recent Via Lactea simulations. As an example of possible form factors, we present a class of models where the necessary momentum dependence arises from interference of GeV mass gauge bosons coupling the dark matter to nuclei. At energies relevant for direct detection experiments these models contain one or two additional parameters beyond the case of a standard WIMP.

---

## 1 Introduction

For several years now, the Dark Matter (DAMA) collaboration has observed an annual modulation in the nuclear recoil event rate at its NaI detector, and the significance of the detection is now at the  $8\sigma$  level [1, 2]. It is striking that the modulation reaches its maximum within a week of June 2nd, when the earth's motion into the galactic dark matter is at its greatest. However, if one supposes that the DAMA signal is to be explained by a weakly interacting massive particle (WIMP) elastically scattering off of nuclei in the detector, then one predicts far too many events to be seen at other experiments. The tension is particularly acute at low nuclear recoil energies, where standard WIMP event rates are expected to increase dramatically.

Although DAMA apparently cannot be reconciled with other experiments within the context of minimal WIMP models (see, for example, [3]), this is not necessarily true in more general scenarios. Essentially, there is no other experiment that is sensitive to the DAMA signal in a model-independent context. In particular, there are three crucial aspects of the DAMA experiment which may be exploited in attempts at an explanation. These are: 1) the masses of the particular nuclei used in the experiments, 2) the fraction of the modulated vs. unmodulated event rate, and 3) the particular ranges of nuclear recoil energies being probed. Recently, inelastic Dark Matter (iDM) [4, 5, 6, 7, 8, 9] has received a great deal of attention for taking advantage of all three through a simple and elegant kinematic mechanism that

easily arises in specific particle physics models. In fact, as the data has improved, few if any other models are consistent with DAMA and all null experimental results. In this paper, we will present an additional class of models as an alternative to iDM, which uses a dynamical rather than a kinematic mechanism.

We will show how our mechanism can arise from a fairly straightforward model where the dark matter interacts with the Standard Model by containing constituents charged under new dark forces that kinetically mix with the photon. In terms of model-building, iDM is clearly simpler than our model. However, we wish to emphasize that model-building dynamical dark matter form factors can be an open direction for explaining DAMA, and there may be a variety of relatively simple alternative models. Thus, in the first part of this paper, we will try to determine in a model independent way how well one can possibly do with a form factor in terms of explaining all of the available data. We will see that the answer depends to an extent on the uncertainties currently present in our understanding of the dark matter halo velocity distribution. The picture works somewhat poorly in the context of the standard halo model, but much better with the results of the Via Lactea numerical simulations. In all cases we find a preferred dark matter mass window, lying in a general range from about 30 GeV up to about 50 GeV, with uncertainties coming from halo assumptions.

The outline of this paper is as follows. In section 2, we will review the general ingredients which go into predictions for direct detection experiments. Section 3 will discuss the motivations for the form factor mechanism, as well as the model independent, best-case-scenarios for the picture. In section 4, we will present specific constructions which yield form factors with the appropriate momentum-dependence. We will note that the models we present simplify considerably in the low energy theory relevant for direct detection experiments. In this limit, the relevant parameters for the models become the mass of the dark matter particle, the overall cross-section, and the relative size of the  $q^4$  term in the form factor compared to the  $q^2$  term (as well as possibly higher-power terms). In this way, the simplest theories we consider have exactly as many free parameters as iDM. Section 5 contains a summary of all of the present experimental data relevant to our analyses, while in section 6 we will use this data to constrain the parameters of our models, as well as give some examples of predicted spectra. Conclusions and future directions will be discussed in section 7.

## 2 Review of Standard Elastic WIMP and Inelastic Dark Matter

Here we will briefly review the standard formalism for direct dark matter detection experiments; for detailed reviews, see e.g. [10, 11]. The rate per unit detector mass per unit recoil energy for dark matter nuclear scattering events is given by the general expression

$$\frac{dR}{dE_R} = N_T \frac{\rho_{\text{DM}}}{m_{\text{DM}}} \int_{v_{\min}} d^3v f(\vec{v}) v \frac{d\sigma}{dE_R}. \quad (1)$$

Here  $N_T$  is the number of target nuclei per unit detector mass, and  $\rho_\chi$  is the local halo density of the dark matter particle, whose mass is  $m_{\text{DM}}$ . The rate depends on the local distribution  $f(v)$  of the dark matter velocity  $v$  relative to the earth. The integral over the velocity distribution depends on the nuclear mass and recoil energy only through the minimum velocity  $v_{\text{min}} = \frac{1}{\mu} \sqrt{\frac{m_N E_R}{2}}$  that a dark matter particle must have in order to result in a nuclear recoil energy of  $E_R$ , where  $m_N$  is the nuclear mass, and  $\mu$  is the dark matter-nucleus reduced mass.

The cross section for a standard WIMP on a nucleus with charge  $Z$  and atomic number  $A$  is given by

$$\frac{d\sigma}{dE_R} = \frac{m_N}{2v^2} \frac{\sigma_p}{\mu_n^2} \frac{(f_p Z + f_n(A - Z))^2}{f_p^2} F_N^2(E_R). \quad (2)$$

where  $\mu_n$  is the dark matter-nucleon reduced mass,  $\sigma_p$  is the dark matter-proton cross section at zero momentum transfer,  $f_n$  and  $f_p$  are the relative coupling strengths to protons and neutrons, and  $F_N$  is the nuclear form factor. We will normalize our results to  $f_n = 0$  throughout, corresponding to the specific models we present. A common parameterization of the nuclear form factor is the Helm form factor

$$F_{\text{Helm}}^2(q) = \left( \frac{3j_1(qr_0)}{qr_0} \right)^2 e^{-s^2 q^2}, \quad (3)$$

where  $s = 1 \text{ fm}$ ,  $r_0 = \sqrt{r^2 - 5s^2}$ ,  $r = 1.2A^{1/3} \text{ fm}$ , and  $q = \sqrt{2m_N E_R}$  is the momentum transfer. A more accurate parameterization comes from the Woods-Saxon form factor, which is the Fourier transform of the Two-Parameter Fermi mass distribution  $\rho(r) = \frac{\rho_c}{e^{(r-c)/a} + 1}$ . We will take the Woods-Saxon form factor for Iodine ( $c = 5.593\text{fm}$ ,  $a = 0.523\text{fm}$ ), Germanium ( $c = 4.45\text{fm}$ ,  $a = 0.592\text{fm}$ ) and Tungsten ( $c = 6.51\text{fm}$ ,  $a = 0.535\text{fm}$ ) [12, 13], and use the Helm form factor for the remaining elements.

Uncertainties in the form of the velocity distribution  $f(v)$  remain significant, as we will discuss in more detail, but a reasonable starting point is that  $f(v)$  in the galactic rest frame is a Boltzmann distribution  $\propto e^{-v^2/\bar{v}^2}$ , with  $\bar{v} = 220\text{km/s}$ , and with a cut-off at the escape velocity  $v_{\text{esc}} = 550\text{km/s} \pm 50\text{km/s}$  [14]. In our analysis, we will take  $v_{\text{esc}} = 600\text{km/s}$ , since this end of the allowed range tends to be more favorable for our models. To obtain our observed velocity distribution, the above expression must be boosted into the Earth's rest frame. The Earth is traveling through the galaxy with velocity  $v_e = v_s + 29.79\text{km/s}(\cos(2\pi(t - t_{\text{JUNE}})\{0.262, 0.504, -0.823\} + \sin(2\pi t - t_{\text{JUNE}})\{-0.960, 0.051, -0.275\}))$ , where the sun's velocity is  $v_s = \{10, 225, 7\}\text{km/s}$ , and we use coordinates with  $\hat{x}$  pointing towards the center of the galaxy,  $\hat{y}$  in the direction of the disc rotation, and  $\hat{z}$  towards the galactic north pole [10, 7]. The magnitude of the Earth's velocity through the galaxy is at a maximum on  $t = t_{\text{JUNE}} = \text{June 2}$ , causing a maximum in the net flux of dark matter particles.

The inelastic dark matter scenario involves a simple generalization of the above such that a small amount of energy  $\delta$ , usually a mass splitting, is lost in the scattering to the dark

sector. The only modification of the above is to increase the minimum velocity by an amount  $\delta/q$ :

$$v_{\min} = \frac{q}{2} \left( \frac{1}{m_{\text{DM}}} + \frac{1}{m_N} \right) + \frac{\delta}{q} \quad (4)$$

The additional contribution means that  $v_{\min}$  gets pushed out to the tail of the velocity distribution for smaller momenta  $q$  and larger dark matter masses  $m_{\text{DM}}$  than in the elastic case. Its form is also very significant:  $\frac{\delta}{q}$  grows at *decreasing*  $q$ , and in fact  $v_{\min}$  has a minimum possible value  $\sqrt{2\delta(m_{\text{DM}}^{-1} + m_N^{-1})}$  that grows with decreasing nuclear mass. This is one of the main original motivations for inelastic dark matter.

Event rates modulate the most over the course of the year for recoils dominated by particles on the tail of the velocity distribution. DAMA is the only experiment looking at a modulation signal, and ideally one way to try to reconcile DAMA with null results at other experiments would be to choose the dark matter mass sufficiently light (e.g. [15, 16, 17, 18, 19]) in order to make  $v_{\min}$  at DAMA sufficiently large. Unfortunately, in the standard WIMP scenario, this means that the event rate at DAMA should rise rapidly as the recoil energy decreases [20], and this does not match the observed spectrum. Furthermore, one faces immediate problems at the Germanium-based CDMS experiment, where the lighter element and lower recoil energies imply lower  $q$  and thus much less kinematic suppression.

Fortunately, both of these problems stem from the sharp rise in the predicted spectrum at low  $q$ , and may be addressed by an additional form factor coming from the dark matter interactions, as we now discuss.

### 3 Overlap in $q^2$

The tension between the apparent signal at DAMA and the direct detection experiments claiming null results becomes clearer through a comparison of their overlap in momentum transfers  $q$ , as shown in Fig. 1. In this paper, we will be considering scenarios in which the cross section eq. (2) is multiplied by an additional function  $F_{\text{DM}}(q)^2$  coming from the dark matter sector. An important aspect of any such additional form factor  $F_{\text{DM}}(q)$  is that it does not depend on the nuclear mass and the recoil energy separately, but only on their product  $m_n E_R = q^2/2$ . As a consequence, any dynamical suppression at lighter nuclei can be completely compensated for by looking at higher energies. Perhaps more importantly, a form factor cannot be used to suppress events at a given experiment in an arbitrary way: the DAMA modulating signal probes values of  $q$  between  $q_i \sim 70$  MeV and  $q_f \sim 120$  MeV, and in this range one therefore has significant constraints on the nature of the form factor. Between  $q_i$  and  $q_f$ , the form factor cannot be too small lest the DAMA signature disappear, whereas outside of  $q_i$  and  $q_f$ , there is no model-independent lower bound.

In practice, one would ideally like the form factor to serve two distinct, but related purposes, alluded to above. First, as noted, one would like it to suppress the scattering rate at

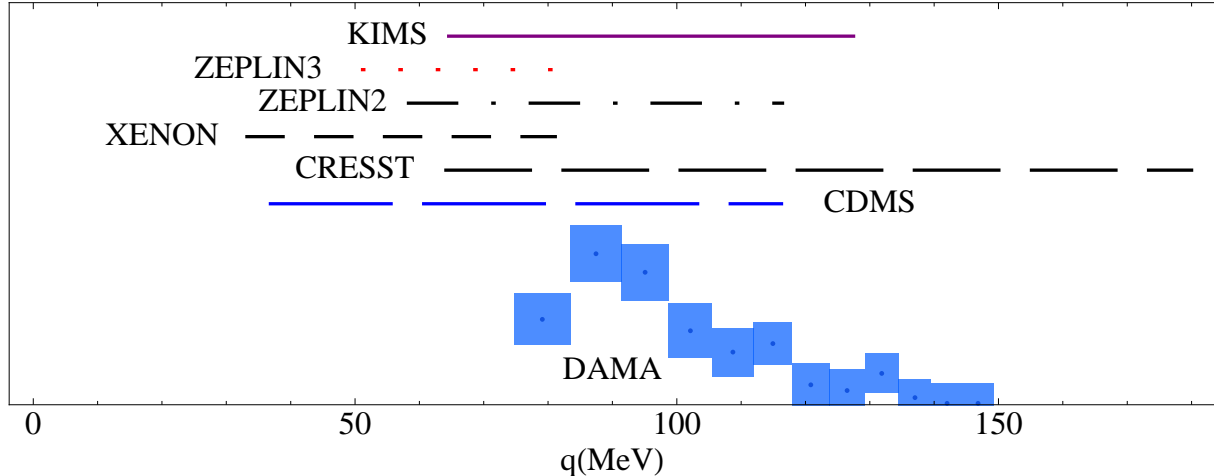


Figure 1: Overlap in  $q$  of the DAMA signal with several null experiments. The height of the null experiments has no particular meaning.

momentum transfers outside of the DAMA range. In addition to this, it should also serve to flatten the spectrum of events observed at DAMA compared to the steep rise at low recoil energies predicted by a standard light elastically scattering WIMP. Both of the above purposes may be served simultaneously by a form factor which falls off appropriately at *low* momentum transfers.

Now, a key point is that the events seen by DAMA between  $q_i$  and  $q_f$  essentially lead to a direct prediction (up to modulation fraction) for the events to be seen at other experiments within that same range of momentum transfers. These predictions are more or less independent of the choice of form factor, and it is therefore not immediately obvious whether they alone are enough to rule out form factor dark matter as an explanation for DAMA. The most basic question we must answer is thus the following: does there exist any function  $F(q)$  for the form factor - which we may take to be zero outside of the range  $q_i < q < q_f$  - which allows for the DAMA modulating signal, but which does not overpredict the number of events to be seen between  $q_i$  and  $q_f$  at other experiments?

Later we will consider explicit models that give rise to form factors, but for the moment we would like to answer this question while being as agnostic as possible about the model-building aspects. Thus we will begin by working with a physically unmotivated form factor, chosen solely with the goal of fitting the DAMA observed spectrum while simultaneously being consistent with the null experiments. To achieve this, we will construct a form factor to explicitly put the signal just below the  $1\sigma$  error bar at DAMA, bin-by-bin<sup>1</sup>. Furthermore, outside the range of the DAMA signal (i.e. below  $q = 80$  MeV), we set the form factor to zero. An example is shown in Fig. 3. To evaluate the consistency of this form factor with experiment, we calculate the probability of the low number of potential signal events

<sup>1</sup>More precisely, we construct the signal to be 80% of the signal-minus- $1\sigma$  rate.

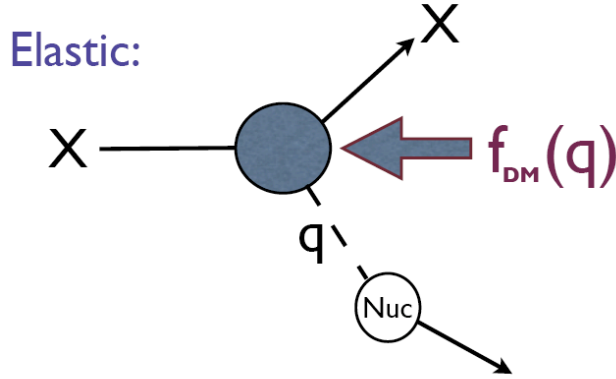


Figure 2: Schematic Feynman diagram for a form factor.

at CDMS and CRESST-II using the *pmax* method [5, 21], which is based on the number of events predicted to have been seen in the gaps between potential events<sup>2</sup>. We also calculate the  $\chi^2$  of the fit at DAMA, which changes with dark matter mass and halo parameters due to the finite escape velocity. In particular, sufficiently large recoil energies necessarily have velocities above  $v_{\text{esc}}$ , and thus the signal is killed by phase space regardless of the size of the form factor. This tends to rule out small dark matter masses. We will take a fairly lax criterion for the probability of the DAMA fit in the lowest 12 bins, calculating only the goodness-of-fit for  $\chi^2$  with 10 degrees of freedom. Of course, currently the form factor has a very large number of free parameters, but we are imagining the best-case scenario where one has constructed a model that automatically gives rise to the desired shape, and the only free parameters are the dark matter mass  $m_{\text{DM}}$  and the overall size of the cross-section  $\sigma_n$ .

The range of masses available depends highly on the choice of dark matter halo model, so let us now take a moment to describe our approach to this additional uncertainty. As we have mentioned, a commonly used simple model is a Maxwell-Boltzmann distribution for the dark matter velocities with a cut-off  $v_{\text{esc}}$  in the galactic rest frame. We will not attempt a systematic analysis of the effect of halo uncertainties, though in light of their effect we believe such an analysis would be very useful. Instead, we will follow [6] and consider two additional halo models, VL<sub>220</sub> and VL<sub>270</sub>, based on the Via Lactea-I simulation [22]. Such an analysis is conservative in that halo parameters are notoriously difficult to constrain and a thorough analysis marginalizing over all halo parameters would open up more of the dark matter parameter space<sup>3</sup>.

The VL<sub>*x*</sub> models are based on a parameterization of the radial and tangential velocity

<sup>2</sup>We present in detail our assumptions about the data from CDMS and CRESST-II in section 5.

<sup>3</sup>We emphasize that the main effect of the Via Lactea halo models will be due to their tighter velocity distributions, and similar qualitative effects would result from Maxwellian distributions with smaller RMS velocities.

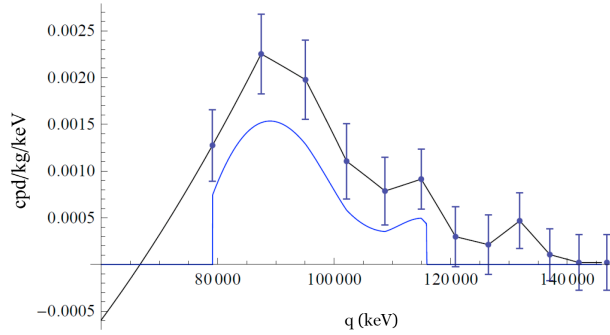


Figure 3: An example of a spectrum from an idealized form factor. The discontinuous drop at low energies is by construction, to suppress all events outside of the DAMA signal range, while the discontinuous drop at high energies arises from the fact the escape velocity  $v_{\text{esc}}$  cuts off the phase space beyond that point.

distributions [3, 6] in the galactic rest frame, fit to Via Lactea simulation results:

$$f(v_R) = \frac{1}{N_R} \exp \left[ - \left( \frac{v_R^2}{\bar{v}_R^2} \right)^{\alpha_R} \right] \quad (5)$$

$$f(v_T) = \frac{2\pi v_T}{N_R} \exp \left[ - \left( \frac{v_T^2}{\bar{v}_T^2} \right)^{\alpha_T} \right] \quad (6)$$

with  $\alpha_R = 1.09$ ,  $\alpha_T = 0.73$ ,  $\bar{v}_R = 0.72\sqrt{-U(r_0)}$ ,  $\bar{v}_T = 0.47\sqrt{-U(r_0)}$ , where  $U(r_0)$  is a normalization parameter. The resulting  $\sqrt{-U(r_0)}$  around  $r_0 \approx 8$  kpc in the Via Lactea-I simulation was 270 km/s; taking this value gives the VL<sub>270</sub> model. If one instead sets  $\sqrt{-U(r_0)}$  to the value 220 km/s in order to obtain a somewhat tighter distribution, then the result is the VL<sub>220</sub> model. Given the uncertainty in the halo parameters and the difficulty in simulating the Milky Way (e.g. including baryons), we believe VL<sub>220</sub> is within the allowed halo model parameter space and is important to include.

The results of our idealized form factor construction are shown for these three different halo models in Fig. 4. One can see that, even with our fairly conservative constraints, there is hardly any region of masses allowed within the standard halo model. The rapid rises in  $\chi^2$  for the fit to DAMA occur when the minimum velocity in an energy bin starts to exceed the bound from the escape velocity, at which point no form factor is capable of reproducing the DAMA signal in that bin. This suggests that a purely dynamical explanation of DAMA is disfavored in the standard halo model<sup>4</sup>. However, there is significantly more room to work

<sup>4</sup>The range of allowed masses is somewhat sensitive to the value of the quenching factor  $q_I$  for iodine recoils at DAMA, as it affects the reconstructed nuclear recoil energy range of DAMA's signal. Here we have taken  $q_I = 0.085$ , but if future improved measurements find it to be lower, then that would move the DAMA spectrum up in recoil energy, thereby weakening the CDMS constraint and strengthening the CRESST constraint. For example, in the standard halo model,  $q_I = 0.08$  opens up the 95% allowed mass

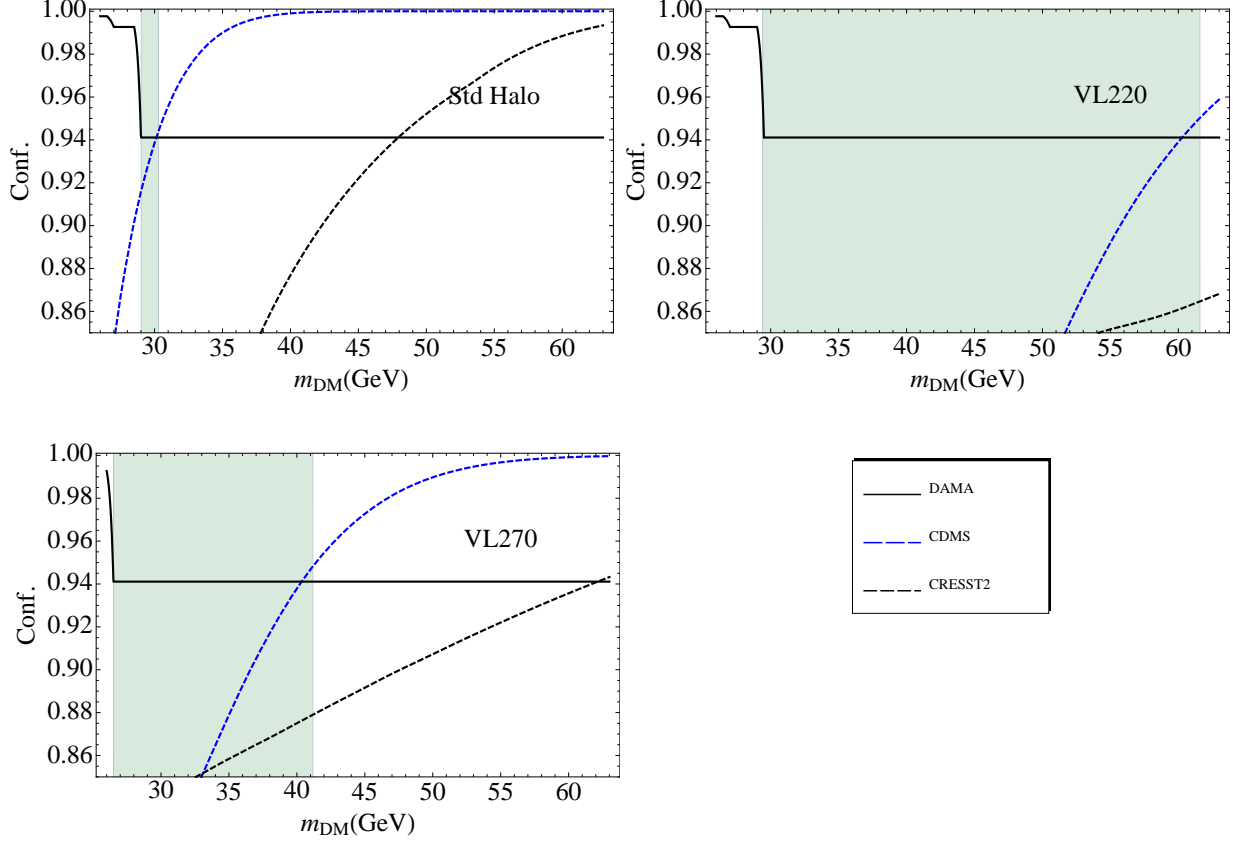


Figure 4: Constraints on idealized form factors for different halo models. For each dark matter mass, we choose a form factor to explicitly match the DAMA spectrum, as described in the text. The confidence levels at DAMA, CDMS and CRESST2 are then plotted. We use a  $\chi^2$  goodness-of-fit test to define the confidence at DAMA, and the *pmax* method for CDMS and CRESST2. The standard halo model leaves very little room for a form factor explanation for all of the data. Highlighted regions have all constraints below 95%.

with in the VL<sub>270</sub> model and, especially, the VL<sub>220</sub> model<sup>5</sup>.

At this point, it is worth re-emphasizing some of the main differences between the iDM mechanism and a dark matter form factor. Because the effect of the splitting  $\delta$  in eq. (4) grows at smaller  $q$ , one obtains a very rapid kinematic shut-down at low DAMA energies, roughly of the form  $\sim e^{-(\delta/q\bar{v})^2}$ . One of the difficulties of model-building a form factor will be to obtain a sufficiently rapid shut-down purely from the dynamics. A more drastic difference is that  $v_{\min}$  is a monotonically increasing function of  $q$  for elastic dark matter but not for inelastic. This makes it generally impossible given the recoil energies and nuclear masses

---

range to  $30.5\text{GeV} \leq m_{\text{DM}} \leq 35.5\text{ GeV}$ . However, at  $q_{\text{I}} = 0.07$ , the CRESST constraint is stronger than CDMS and the mass range shrinks to  $33\text{GeV} \leq m_{\text{DM}} \leq 35\text{ GeV}$ .

<sup>5</sup>We have checked that scattering off of sodium does not work in any of the three halo models we consider for any range of dark matter masses.



at DAMA and CDMS to choose parameters so that there are *no* events at CDMS while simultaneously maintaining the DAMA signal. However, as has been noted in the literature, this is a possibility for inelastic dark matter if the splitting  $\delta$  is chosen sufficiently carefully. We can sharpen this prediction somewhat by considering the minimum number of events predicted at CDMS by our idealized form factor in the 95% goodness-of-fit DAMA region (i.e.  $\chi^2_{\text{DAMA}} < 18.3$ ). This number is proportional to the effective exposure  $\epsilon_{\text{CDMS}}$  at future CDMS runs, so that

$$N_{\text{CDMS,min}} = r_{\text{CDMS,min}} \frac{\epsilon_{\text{CDMS}}}{200\text{kg day}}, \quad (7)$$

where we find that  $r_{\text{CDMS,min}} \approx 4.4, 1.1$ , and  $2.2$  for the standard halo, VL<sub>220</sub>, and VL<sub>270</sub> models, respectively.

## 4 Models

Here we present models leading to a form factor which is consistent with present data. One very simple possible form factor, which is relatively generic at sufficiently low energies, is  $F(q) \propto q^2$ . Such an interaction results in a factor of only  $q^4$  in the event rate, and leads to insufficient suppression of events at null experiments. We are thus lead to introduce a mechanism to further reduce events outside the DAMA region.

Our basic idea is to have multiple gauge bosons coupling regular matter to dark matter which then naturally interfere with one another. In particular, we will examine two models. The first describes two gauge bosons and leads to an effective form factor

$$F_{2GB}(q^2) \sim \left( \frac{g_1^2 q^2}{q^2 + m_1^2} - \frac{g_2^2 q^2}{q^2 + m_2^2} \right). \quad (8)$$

The second model includes three gauge bosons, leading to

$$F_{3GB}(q^2) \sim \left( \frac{g_1^2 q^2}{q^2 + m_1^2} - 2 \frac{g_2^2 q^2}{q^2 + m_2^2} + \frac{g_3^2 q^2}{q^2 + m_3^2} \right). \quad (9)$$

In both cases, we will see that the models possess natural regions in parameter space where there is a custodial symmetry relating the gauge boson masses. In those regions, the analysis of the models simplifies. Specifically, choosing all  $m_i$  to be near a GeV, at momenta of interest ( $q \ll m_i$ ),

$$\begin{aligned} F_{2GB}(q^2) &= c_2 q^2 (q^2 - q_0^2) \\ F_{3GB}(q^2) &= c_3 q^2 (q^2 - q_1^2)(q^2 - q_2^2). \end{aligned} \quad (10)$$

Here, the parameters  $q_i$  are of order 10 MeV, while the  $c_i$  are absorbed into the overall crosssection. Obtaining a crosssection of the appropriate size in both cases requires  $\Lambda, m_i \sim \text{GeV}$ . Therefore, as far as the direct detection experiments are concerned, the two and three gauge boson models contain two and three parameters, respectively.

## 4.1 A two gauge boson model

Consider two massive gauge bosons  $A_\mu^{(1,2)}$  which mix with hypercharge with opposite signs.

$$\mathcal{L} = \epsilon \left( g_1 F_{\mu\nu}^{(1)} - g_2 F_{\mu\nu}^{(2)} \right) B^{\mu\nu} \quad (11)$$

Such a mixing can arise, for example, from integrating out two heavy fields each of which couples to one of the gauge bosons and to hypercharge with charges chosen appropriately.

We assume that the dark matter particle is not charged under the gauge bosons, but that it may be made of constituents that are charged. Consequently, it develops higher-dimensional interactions with both gauge bosons. If it is a scalar, the leading higher-dimensional interactions take the form

$$\mathcal{L} = i \left( \frac{g_1}{\Lambda^2} F_{\mu\nu}^{(1)} + \frac{g_2}{\Lambda^2} F_{\mu\nu}^{(2)} \right) \partial_\mu X^* \partial_\nu X. \quad (12)$$

Here  $X$  is the dark matter particle and  $\Lambda$  is characteristic of its size. Thus, the exchange of the two gauge bosons between the dark matter particle and the protons in nuclei will lead to the form factor of Eq.(8).

Let us now discuss how the gauge bosons obtain their masses. As mentioned, the form factor simplifies in the limit that a custodial symmetry relating the gauge boson masses is weakly broken. We will therefore describe the Higgs fields and their potential with that in mind. Consider a complex doublet,  $\Phi = (\phi_1, \phi_2)$ . The custodial symmetry is an  $SO(2)$  rotation of  $\phi_1$  into  $\phi_2$ .  $\Phi$  couples to the gauge bosons as

$$D_\mu \Phi = \left( \partial_\mu - i \frac{g_1}{2} A_\mu^{(1)} - i \frac{g_2}{2} A_\mu^{(2)} \sigma_3 \right) \Phi. \quad (13)$$

We now turn to the Higgs potential. Let us assume in the following that the only source of breaking of the  $SU(2)$  symmetry acting on  $\Phi$  comes from interactions with  $A_\mu^{(2)}$ , and that the dark sector interactions respect a charge conjugation symmetry (exchanging  $\phi_1$  and  $\phi_2$ ) which takes  $A_\mu^{(2)} \rightarrow -A_\mu^{(2)}$ . With these symmetries, the  $\Phi$  potential takes the form

$$V(\Phi) = -m^2 \Phi^\dagger \Phi + \lambda (\Phi^\dagger \Phi)^2 + y (\Phi^\dagger \sigma_3 \Phi)^2. \quad (14)$$

If  $y > 1$ , at the minimum  $\Phi^\dagger \sigma_3 \Phi = 0$ . This ensures that the gauge boson mass matrix is diagonal and that there is an  $SO(2)$  custodial symmetry relating the gauge boson masses, such that  $m_{1,2} = g_{1,2} v$ . Including terms in the potential which violate the charge conjugation symmetry would make this potential generic, resulting in general gauge boson masses. For our purposes, however, it is useful to assume there is only a small violation of the above custodial symmetry, such that  $\frac{m_1^2}{g_1^2} - \frac{m_2^2}{g_2^2} = (\delta m)^2$ . Such a violation could come, for instance, from the above mixing of the gauge bosons with hypercharge (which violates the charge conjugation symmetry at order  $\epsilon^2$ ). In this case, the size of  $(\delta m)^2$  would depend on additional physics such as the cutoff scale of the  $\Phi$  theory,  $(\delta m)^2 \sim \frac{\epsilon^2}{16\pi^2} \Lambda_{\text{cutoff}}^2$ . One can imagine other sources for  $(\delta m)^2$  as well, and we therefore leave it as a free parameter. Thus, in the limit of

interest, where  $q^2 \ll m_{1,2}^2$ , the form factor is approximated by

$$F_{2GB}(q^2) \sim \frac{q^2}{v^4} \left( \frac{g_1^2 - g_2^2}{g_1^2 g_2^2} q^2 - (\delta m)^2 \right) \equiv c_2 q^2 (q^2 - q_0^2). \quad (15)$$

We note that besides the constant  $c$  that can be reabsorbed into the total cross-section, the only relevant parameter for dark matter detection experiments is  $q_0$ .

## 4.2 A three gauge boson model

One can also consider extending the above scenario to include an additional gauge boson which mixes with hypercharge. The interference between the three gauge bosons can naturally achieve further suppression of the cross-section at low momentum transfer. The resulting model is similar to the model above, but with an  $SO(3)$  custodial symmetry instead. As before, the three gauge bosons mix with hypercharge,

$$\mathcal{L} = \epsilon \left( g_1 F_{\mu\nu}^{(1)} - 2g_2 F_{\mu\nu}^{(2)} + g_3 F_{\mu\nu}^{(3)} \right) B^{\mu\nu}. \quad (16)$$

Such a mixing can be obtained by integrating out three heavy fields, each charged under hypercharge and under only one of gauge bosons. All heavy fields have the same charge under their respective gauge bosons, and charges  $+1$ ,  $-2$ , and  $+1$  under hypercharge.

The dark matter particle couples to the gauge bosons through the leading higher-dimensional interactions,

$$\mathcal{L} = i \left( \frac{g_1}{\Lambda^2} F_{\mu\nu}^{(1)} + \frac{g_2}{\Lambda^2} F_{\mu\nu}^{(2)} + \frac{g_3}{\Lambda^2} F_{\mu\nu}^{(3)} \right) \partial_\mu X^* \partial_\nu X. \quad (17)$$

Hence, gauge boson exchange results in the effective form factor of eq.(9).

We will again concentrate on a version of this model with approximate custodial symmetry. To that end, we take the Higgs field,  $\Phi$ , to be a four of  $SU(4)$ , charged under the gauge bosons as

$$D_\mu \Phi = \left( \partial_\mu - ig_i A_\mu^{(i)} Q_i \right) \Phi. \quad (18)$$

Here, the charges,  $Q_i$  are embedded in  $SU(4)$  as

$$Q_1 = \begin{pmatrix} \mathbb{1} & \\ & \mathbb{1} \end{pmatrix}, Q_2 = \begin{pmatrix} \mathbb{1} & \\ & -\mathbb{1} \end{pmatrix}, Q_3 = \begin{pmatrix} \sigma_3 & \\ & \sigma_3 \end{pmatrix}, \quad (19)$$

where  $\mathbb{1}$  is the two by two identity matrix. Assuming that the only interactions breaking the  $SU(4)$  symmetry are the gauge interactions, a general potential respecting all manner of charge conjugation symmetries is

$$V(\Phi) = -m^2 \Phi^\dagger \Phi + y_i (\Phi^\dagger Q_i \Phi)^2 + \tilde{y} (\Phi^\dagger Q_2 Q_3 \Phi)^2. \quad (20)$$

If  $y_i, \tilde{y} > 0$ , then at the minimum an  $SO(3)$  custodial symmetry acting on the gauge boson masses will be respected, and  $m_i = g_i v$ . This custodial symmetry will be violated at order  $\epsilon^2$ . We thus define  $(\delta m)^2 = \frac{2m_2^2}{g_2^2} - \frac{m_1^2}{g_1^2} - \frac{m_3^2}{g_3^2}$ .

In order to obtain a simplified version of this model at low  $q$ , we will further require that the three gauge bosons unify at some scale  $M_U$ . For instance, the unified group can be  $SO(8) \supset SU(4) \times U(1)$ , with  $\Phi$  transforming as the eight of  $SO(8)$ . Therefore,  $g_i(M_U) = g_U$ . Below  $M_U$ , we assume that the matter content is such that the running splits the couplings, but maintains the relation  $\frac{1}{g_1^2} - \frac{2}{g_2^2} + \frac{1}{g_3^2} = 0$ . This is possible if for example there are twice as many fermions charged under only  $U(1)_1$  as under only  $U(1)_2$ , with no new matter (besides  $\Phi$ ) charged under  $U(1)_3$ . Threshold effects would then account for a violation of the relation between couplings, so that  $\frac{1}{g_1^2} - \frac{2}{g_2^2} + \frac{1}{g_3^2} \equiv \delta g \lesssim \frac{1}{100}$ . Consequently, at  $q \ll m_i$ ,

$$F_{3GB}(q^2) \sim \frac{q^2}{v^6} \left[ \left( \frac{1}{g_1^4} - \frac{2}{g_2^4} + \frac{1}{g_3^4} \right) q^4 - \delta g v^2 q^2 + (\delta m)^2 v^2 \right] \equiv c_3 q^2 (q^2 - q_1^2)(q^2 - q_2^2). \quad (21)$$

We note that choosing  $\Lambda_{\text{cutoff}} \sim 4\pi v$  naturally gives  $(\delta m)^2 v^2 \sim 10^{-6} v^4$ , which is the appropriate size for  $q_i^4$  (assuming all couplings are of order one).

## 5 Null Experiments and Analysis

We will briefly describe the null experiments whose constraints we include and the assumptions that go into our analysis. We have attempted to follow the analysis assumptions of [5] in order to make the comparison with inelastic dark matter transparent. Summary tables of the assumptions at each experiment are 1,2, and 3. Tables 2 and 3 show the relevant data used in our analysis concerning the various null experiments. Generally, these experiments see some set of unexplained events whose energies are indicated in table 3, and in our analysis we have allowed ourselves to interpret these as potential dark-matter-induced nuclear recoils. The energies listed in this table are actual nuclear recoil energies, and have thus been obtained by dividing the detected energy by a quenching factor where appropriate. In all null experiments in which individual potential events are published, we calculate the constraints using the *pmax*, or “maximum gap”, value [21]. This is the probability, given a specific model, of an experiment having seen no events in the gap between any two adjacent potential events. When the number of observed events is very low, this method is very sensitive to, for example, non-blind cuts on events, since a single additional event in the middle of a gap can drastically increase the likelihood.

### 5.1 DAMA

We take for the DAMA signal the published modulation amplitudes from Fig. 9 of [1], which we summarize in Table 1. The energy shown is that observed in the detector, and is smaller than the actual nuclear recoil energy by an amount given by the “quenching factor”. For Iodine scattering events in a NaI crystal, we take the quenching factor to be 0.085. We implement scattering off Iodine only, as our form factor suppresses events scattering off of Sodium. We calculate the modulation amplitude as half of the difference between the event rate on June 2 and Dec. 2. To obtain our confidence limits on our models from DAMA, we

Bin Energy (keVee)	Modulating Amplitude (cpd/kg/keVee)		
2.25 $\pm$ .25	.015 $\pm$ .0045	Bin Energy (keVee)	Amplitude (cpd/kg/keVee)
2.75 $\pm$ .25	.027 $\pm$ .0050		
3.25 $\pm$ .25	.023 $\pm$ .0050	3.5 $\pm$ 1.	.11 $\pm$ .099
3.75 $\pm$ .25	.013 $\pm$ .0048	4.5 $\pm$ 1.	.11 $\pm$ .078
4.25 $\pm$ .25	.0093 $\pm$ .0043	5.5 $\pm$ 1.	.027 $\pm$ .069
4.75 $\pm$ .25	.011 $\pm$ .0038	6.5 $\pm$ 1.	.074 $\pm$ .054
5.25 $\pm$ .25	.0035 $\pm$ .0038	7.5 $\pm$ 1.	-.0008 $\pm$ .037
5.75 $\pm$ .25	.0025 $\pm$ .0038	8.5 $\pm$ 1.	.051 $\pm$ .036
6.25 $\pm$ .25	.0055 $\pm$ .0035	9.5 $\pm$ 1.	.051 $\pm$ .027
6.75 $\pm$ .25	.0013 $\pm$ .0033	10.5 $\pm$ 1.	.065 $\pm$ .026
7.25 $\pm$ .25	.00025 $\pm$ .0035		
7.75 $\pm$ .25	.00025 $\pm$ .0035		

Table 1: Left: amplitude of the modulating part of the DAMA signal, divided into 0.5keVee bins. Right: amplitude of the measured rate at KIMS, in 1.0 keVee bins.

find the best  $\chi^2$  at a fixed mass and show contours of  $\chi^2 = \chi^2_{\min} + 4.61(9.21)$  for 90% (99%) confidence.

## 5.2 CDMS

We combine the CDMS data from the three runs in [23, 24, 25], for a total of 174.4 kg days after including their published 30% acceptance rates on a standard WIMP. The first run had 20 kg-days and ran from Oct. 11 - Jan 11, the second had 34 kg-days and ran from Mar. 25-Aug 8, and the latest five-tower run (which saw no events) had 121 kg-days and ran from Oct. to July.

## 5.3 CRESST-II

We combine the CRESST-II data from the 2004 run [26] and the latest commissioning run [27] from 2007. The '04 run ran from Jan. 31 - Mar. 23, had 20.5 kg-days of exposure, and looked at recoil energies of 12-50 keV. The '07 run ran from Mar. 27 - July 23, had 47.9 kg-days of exposure, and looked at 12-100 keV. Both runs had very mild cuts leading to a 90% acceptance rate. The '04 run had two detectors, one of which (JULIA) saw four events, and the other of which (DAISY) saw no events using the published quenching factors, and one events after varying the quenching factors within their published uncertainties. The '07 run also had two detectors, which saw a total of seven events. We should note that the *pmax* constraints from the '07 run alone are much stronger than the constraints from the combined '04/'07 analysis, but given that the '07 run was non-blind we follow [5, 28] and take all the

Experiment	Element	Dates	Effective Exposure (kg days)	Signal Window (keV)
CDMS	Ge	Oct. 2- July 31	174.4	10 - 100
XENON	Xe	Oct. 1 - Feb. 28	122*	2 - 70
CRESST-II, '04	CaWO <sub>4</sub>	Jan. 31 - Mar. 23	18.5	12 - 50
CRESST-II, '07	CaWO <sub>4</sub>	Mar. 27 - July 23	43.1	12 - 100
ZEPLIN-II	Xe	May 1 - June 30	112.5	13.9 - 55.6
ZEPLIN-III	Xe	Feb. 27 - May 20	126.7	10.7 - 30.2
KIMS	CsI	see text	N/A	20.6 - 65.4

Table 2: Elements, dates, effective exposures and signal windows for the null experiments. The exposures have been listed here only after efficiencies and cuts have been taken into account (it is still necessary, however, to multiply by the fraction of target nuclei in the detector material). \*XENON effective exposure is approximate, since the efficiencies and acceptance rates are energy-dependent. This was taken into account in our analysis.

CRESST-II data together.

## 5.4 XENON

For XENON10 [29], we take the published data of the recent reanalysis [30] in the extended range 2.0-70 keV. The experiment ran from Oct. 1- Feb 28. and had a total of 316 kg-days. We take the published energy-dependent acceptance rates and efficiencies.

## 5.5 ZEPLIN-II and ZEPLIN-III

ZEPLIN-II is a Xenon based experiment with 225 kg-days of effective exposure after cuts are applied, and in addition there is a recoil detection efficiency of 50%. We take the quenching factor to be 0.36, and the 29 events from Fig. 8 of [31]. We take all events as potential signal in calculating our limits.

ZEPLIN-III ran in 2008 from Feb. 27 - May 20 and observed only 7 events between 10.7-30.2 keV [32].

## 5.6 KIMS

KIMS [33] had four CsI(Tl) crystals looking in the range 3-11 keVee, two of which ran roughly year-round and two of which ran between June and March. We take the weighted average over all four crystals to obtain the measured rate and error, shown in table 1. We use the parameterization of the quenching factor from [6]:

$$q_{CsI}(E_R) = \frac{0.175e^{-E_R/137}}{1 + 0.00091E_R}, \quad (22)$$

Experiment	Events (keV)
CDMS	10.5, 64
XENON	15.8, 23.8, 24.1, 25.9, 32.2, 33.7, 38.7, 39.2, 40.1, 43.3, 43.6, 51.6, 62.3
CRESST-II '04	13, 18.5, 22.5, 24, 33.5
CRESST-II '07	16.7, 18.03, 33.09, 43, 43, 43, 63
ZEPLIN-II	13.9, 15.3, 16.7, 16.7, 16.7, 18.1, 19.5, 19.5, 20.9, 20.9, 22.2, 22.2, 23.6, 27.8, 27.8, 29.2, 30.6, 33.4, 37.5, 37.5, 38.9, 41.7, 43.1, 44.5, 44.5, 48.7, 50.0, 50.0, 54.2
ZEPLIN-III	14.6, 17.2, 20.8, 22.9, 23.4, 25.1, 28.1

Table 3: Unexplained events observed by the null experiments, listed by nuclear recoil energy in keV.

and define the constraint as the requirement that the total scattering off Cesium and Iodine not be more in any of the first five bins (3-8 keVee) than the measured rate plus 1.64 times the error.

## 6 Results

Exclusion plots are shown in Figs. 5 and 6<sup>6</sup> for the two- and three-gauge boson (2GB and 3GB) models, respectively. In order to reduce the parameter space and thus simplify the contour plots, we have taken both nodes in the 3GB model to be at  $q_1 = q_2 \equiv q_0$ ; the improvement in consistency with the null experiments by varying them separately is relatively small. We have checked that in each case, the constraint from KIMS can be neglected since it is weaker than both the CDMS and CRESST-II constraints, and in fact its 95% constraint curve does not cut out any of the DAMA 90% preferred region<sup>7</sup>. The DAMA inner (outer) contours are shown at 90% (99%), and the  $pmax$  constraints for the null experiments are shown at 99% (95%) for the 2GB (3GB) model<sup>8</sup>. There is a fairly strong dependence of the limits on the dark matter mass, both at DAMA and at the null experiments. As discussed in section 3, sufficiently low masses put the DAMA signal above  $v_{esc}$  and thus are excluded. On the other hand, sufficiently high masses cause the velocity dispersion to flatten out at low recoil

<sup>6</sup>The dark matter-proton cross-section  $\sigma_p$  now involves the form factor, and so is a function of  $q$ . We therefore have defined  $\sigma_{p,100\text{MeV}}$  in the following way:  $\sigma_p = \sigma_{p,100\text{MeV}} F_{\text{DM}}^2(q)$ , where  $F_{\text{DM}}(q)$  is normalized e.g. as  $q^2(q^2 - q_1^2)(q^2 - q_2^2)/(100\text{MeV})^6$ .

<sup>7</sup>We note that in our models the constraint from comparing the unmodulated DAMA signal to the modulated DAMA signal is an even weaker constraint on the modulation fraction than KIMS is, and so may also be neglected. The danger of overpredicting the unmodulated signal in low energy bins  $E_R < 20$  keV is avoided as we predict the spectrum to decrease at low energies.

<sup>8</sup>The reason for this difference is that the DAMA 99% preferred region for the 2GB model is just barely excluded at 95% by our analysis. We hope this will not cause too much confusion.

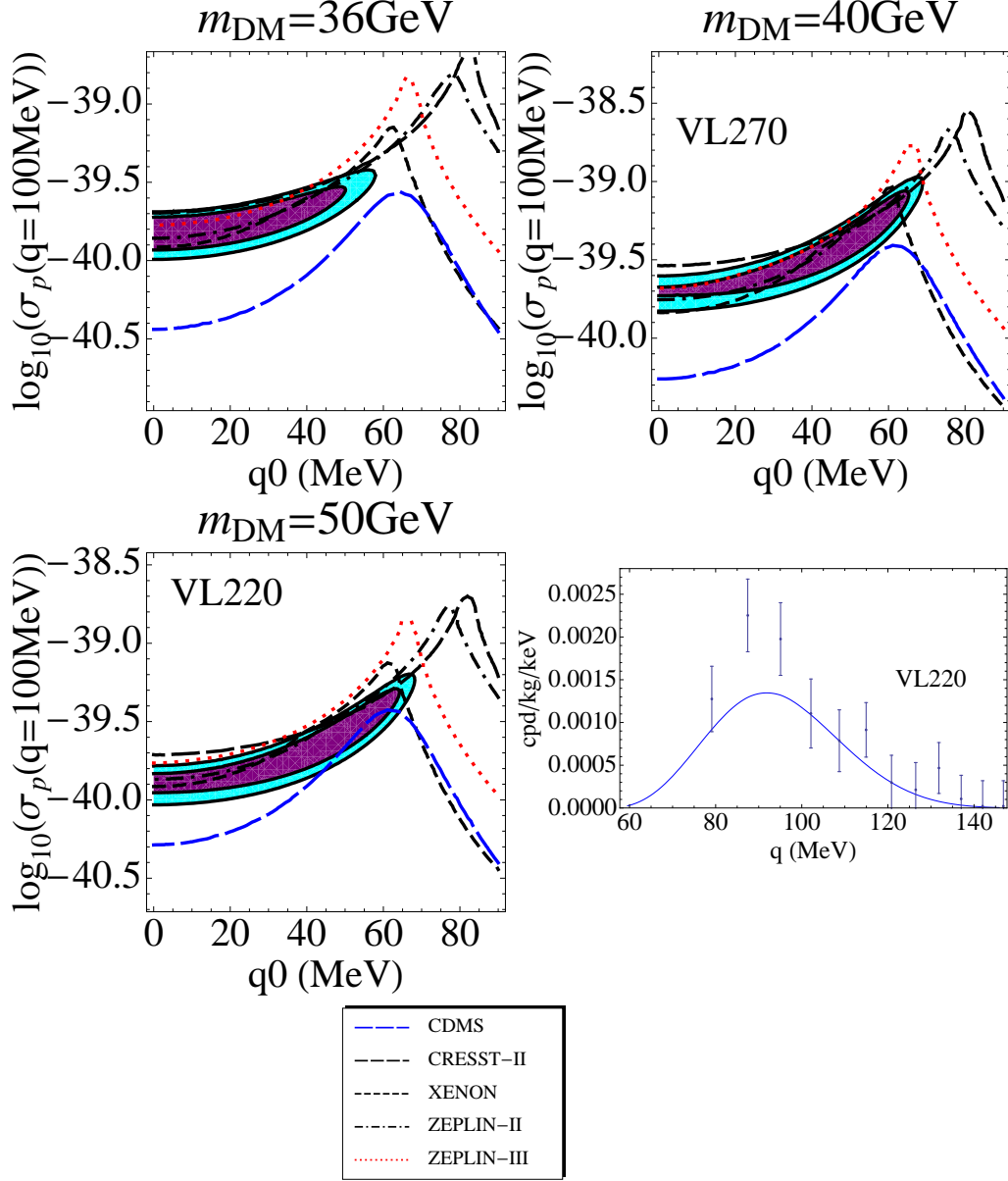


Figure 5: Exclusion plots for the two-gauge-boson (2GB) model. Confidence limits from DAMA are shown in purple (light blue) for 90% (99%), all other confidence limits are 99%. The spectrum at DAMA is shown for a benchmark point with VL<sub>220</sub>; see table 4 for the model parameters.  $\sigma_p$  is taken in units of  $\text{cm}^2$ .

energies. In our specific models, the lower energy bins are too suppressed by the form factor and the spectrum is incorrectly distorted. On top of this, larger masses do not lead to a large enough modulation fraction at DAMA in order to evade the null constraints. In Figs. 5 and 6, we have chosen masses from around the regions where the constraints are weakest.



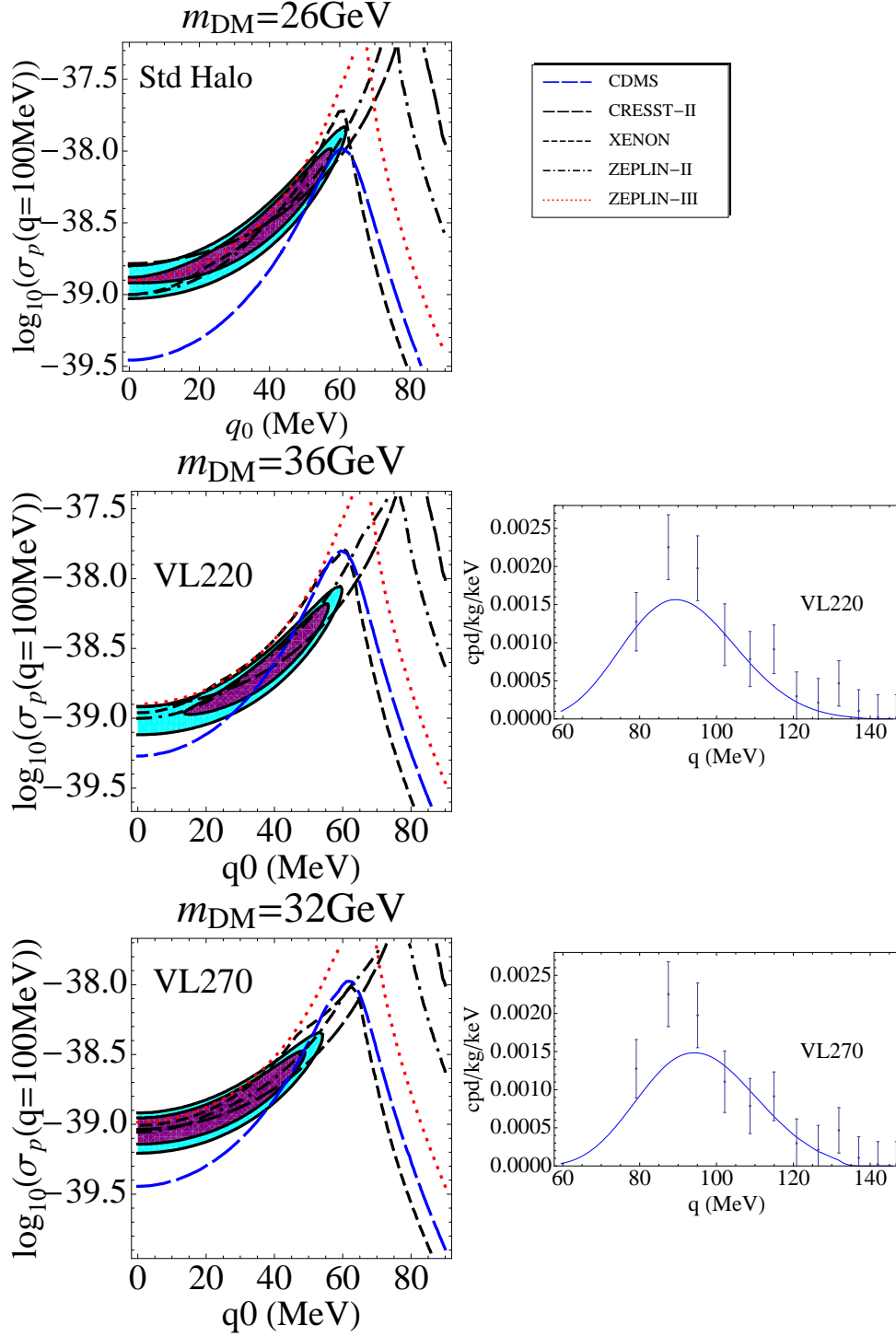


Figure 6: Exclusion plots for the three-gauge-boson model (3GB) with both nodes taken at the same value  $q_1 = q_2 \equiv q_0$  for simplicity. Confidence limits from DAMA are shown in purple (light blue) for 90% (99%), all other confidence limits are 95%. The spectrum at DAMA is shown for two benchmark points; see table 4 for the model parameters.

The DAMA preferred region for the 2GB model is excluded by our analysis at 95% confidence. In all cases, the culprit is CDMS, due to the fact that the form factor does not fall quite rapidly enough below the DAMA signal region. We find though that at  $VL_{220}$  the 95% CDMS line just barely excludes the DAMA preferred region, and there are still a number of uncertainties (e.g. in quenching factors, energy resolution) that we have not attempted to take into account. The situation is much better in the 3GB model, where we show 95% exclusion limits. In the standard halo model, no parameter space is left at 90%, but for the Via Lactea models the DAMA preferred region is just barely allowed by our exclusion limits. The CDMS constraint is considerably weaker for the 3GB model, due to the sharper fall-off of the form factor at energies just below the DAMA signal. As one might have expected, the other experiments with a sizeable range below the DAMA signal (XENON, ZEPLIN-II, and ZEPLIN-III) have also gotten weaker relative to CRESST-II. One can clearly see the effect of the node  $q_0$  as it passes through the bulk of each individual experiment, removing the predicted events in that region. For  $q_0$  above about 70 MeV (60 MeV) in the 2GB (3GB) model, however, the node starts to suppress the DAMA signal, whereas ideally the form factor will be more or less set in this region by the DAMA spectrum. Around  $q_0 \sim 80$  MeV, the CRESST-II signal is drastically suppressed by the node. Thus the trend in both models is for the lower- $q$  experiments to dominate the constraints at smaller  $q_0$ , whereas for  $40 \text{ MeV} \lesssim q_0 \lesssim 70 \text{ MeV}$ , they are suppressed and CRESST-II becomes the dominant constraint.

The halo model with the most open parameter space is in all cases  $VL_{220}$ . The first major effect of the smaller  $\bar{v}$  at  $VL_{220}$  is to tighten the velocity distribution. This allows for larger dark matter masses without sacrificing the necessary modulation fraction. Additionally, larger masses effectively push the escape velocity cut-off to higher recoil energies at DAMA, improving the fit to the upper energy bins. Finally, it is important to note that despite the tighter distribution at higher energies, the distribution in the lab frame is still relatively flat below the earth's velocity, as the velocity of such events are dominated by the earth's contribution rather than the halo fluctuations. Given how much a modest change (18.5%) in  $\bar{v}$  can affect the allowed parameter space, it is clearly an important issue to understand the experimentally and theoretically allowed range of parameter space for halo models, so that it would be possible to more systematically include all such uncertainties in setting exclusion limits. In the absence of such an analysis, the precise meaning of exclusion limits is not entirely clear.

The value of  $\chi^2$  for the DAMA 90% and 99% contours depends on the minimum  $\chi^2$  for each plot, so it can be helpful to know this value. For the 2GB (3GB) model,  $\chi_{\min}^2 = 4.6, 4.7, 4.7(9.8, 5.0, 5.24)$  for the standard halo,  $VL_{220}$ , and  $VL_{270}$  plot, respectively. In all cases,  $\chi_{\min}^2$  is below  $10 = 12 - 2$ , as appropriate for 12 DAMA bins and 2 free parameters ( $\sigma_p$  and  $q_0$ ). Given the strong dependence of the fits on  $m_{\text{DM}}$ , it is possible that the  $\chi^2$  distribution for our models more closely follows a distribution with three free parameters, in which case our  $\chi_{\min}^2$  is still sufficiently small at  $VL_{220}$ ,  $VL_{270}$ , but the DAMA contours will be larger. In this sense also, our analysis is conservative.

In table 4, we show three benchmark models, one for the 2GB model with the  $VL_{220}$  and

Halo Model	DM Model	$m_{\text{DM}}$	$\chi^2_{\text{DAMA}}$	$\sigma_{p,100\text{MeV}}$	$p_{\text{CDMS}}$	$p_{\text{CRESST}}$
VL <sub>220</sub>	2GB ( $q_0 = 50\text{MeV}$ )	50 GeV	11.8	$2.34 \times 10^{-40}\text{cm}^2$	0.97	0.89
VL <sub>220</sub>	3GB ( $q_1 = 42.5, q_2 = 38\text{MeV}$ )	36 GeV	8.9	$2.00 \times 10^{-39}\text{cm}^2$	0.90	0.90
VL <sub>270</sub>	3GB ( $q_1 = 50, q_2 = 37.5\text{MeV}$ )	32 GeV	10.3	$2.10 \times 10^{-39}\text{cm}^2$	0.94	0.95
”	”	”	14.9	$1.79 \times 10^{-39}\text{cm}^2$	0.90	0.90

Table 4: Our three benchmark points. We also indicate what the constraints on the 3GB(VL<sub>270</sub>) benchmark point would be if a slightly smaller overall cross-section  $\sigma_{p,100\text{MeV}}$  were chosen.

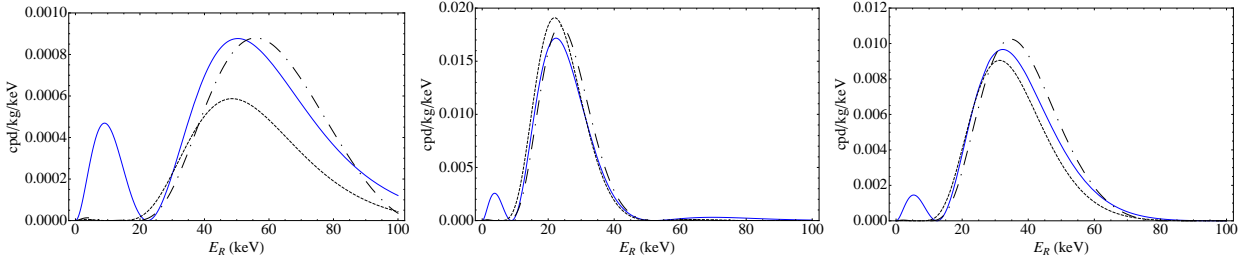


Figure 7: Predicted spectra at Ge (left), W (center) and Xe (right) for the three benchmark points in table 4. We have chosen the time of year to correspond to the dates of CDMS, CRESST-II '07, and ZEPLIN-III, respectively. The 2GB(VL<sub>220</sub>), 3GB(VL<sub>220</sub>), and 3GB(VL<sub>270</sub>) models are shown in solid, dashed, and dot-dashed.

two for the 3GB, one for each VL<sub>x</sub> model, along with their statistical constraints from CDMS and CRESST-II. Note that the null constraints are within 97% for the 2GB model and within 95%(90%) for the 3GB, VL<sub>270</sub>(VL<sub>220</sub>) model. We have also shown in table 4 the constraints on the 3GB(VL<sub>270</sub>) model using a slightly larger value for the cross-section  $\sigma_{p,100\text{MeV}}$ , because such a cross-section would be permitted by a goodness-of-fit  $\chi^2$  test. More precisely,  $\chi^2$  for the fit to DAMA in the new 3GB(VL<sub>270</sub>) model is 14.9, which corresponds to a probability of 86.4% for 10 degrees of freedom, and 90.6% for 9 degrees of freedom. It is, however, just outside the 99% contour  $\chi^2 = \chi^2_{\text{min}} + 9.21 = 14.4$ , which underscores that the constraints are sensitive to the statistical assumptions being made. Finally, we also show in Fig. 7 the predicted spectra for our three benchmark points at CDMS and CRESST-II.

## 7 Discussion and Future Directions

In this paper, we have discussed the possibility of using a dynamical form factor to reconcile the DAMA annual modulation signature with the null results of other direct detection experiments. We have shown that, independent of specific model assumptions, such a form factor can in fact be consistent with all available data. The picture works to varying degrees

depending on the assumptions one makes concerning the distribution of velocities in the dark matter Halo.

An important question is how one might distinguish this scenario from that of inelastic dark matter. For this purpose, probably the most important indicator would be in the energy spectra to be seen at future runs of the various direct detection experiments.

As discussed in section 3, independent of model details, form factor dark matter leads to a prediction for the events to be seen at any direct detection experiment within the range of momenta probed by DAMA. Although this prediction depends somewhat on the dark matter mass, some non-trivial event rates will always be present. Inelastic dark matter, on the other hand, has a bit more flexibility in this regard: due to the form eq. (4) of the minimum velocity for inelastic scattering, it is possible to choose parameters such that  $v_{\min}$  is always above the escape velocity at CDMS but below the escape velocity at DAMA in the energy region of the modulation signal [4, 5]. The result is that inelastic dark matter may be consistent with possibilities such as zero events at future runs of CDMS, a situation which would rule out a pure form factor.

In contrast to this, there are certain aspects of the form factor setup which are actually more flexible than in the inelastic case: inelastic dark matter makes a firm prediction that all experiments should find zero events at momenta smaller than a particular cutoff  $q_{\min} \sim \frac{\delta}{v_{\text{esc}} + v_e}$ , which must be set approximately to the lower end of the DAMA spectrum. A general form factor, on the other hand, could accomodate such events if they were to be seen.

Further differences between the predictions of inelastic and form factor dark matter could become relevant after large amounts of data have been collected. In particular, details of the energy dependence of the fraction of modulating events could be used to differentiate the two pictures, but only with large amounts of statistics. It is also possible that future directional detection experiments could provide an additional handle [8]. Finally, although collider signatures for the general form factor scenario are model dependent, the specific setups discussed in section 4 could lead to events at low energy  $e^+e^-$  colliders of the types discussed in [34, 35].

There are a wide variety of future directions to pursue within the general framework we have discussed in this paper. Of course, we hope that future simulations of the galactic halo, including baryons, will yield a more precise picture for the structure of the dark matter velocity distribution. At the present level of understanding, uncertainties in this distribution have a significant impact on the possible viability and allowed parameter ranges for not only form factor dark matter, but for essentially any proposed explanation for the DAMA annual modulation signature.

From the particle physics side, it would certainly be interesting to try to write down additional types of models leading to form factors with the general features discussed in section 3. In this paper we considered a simple “proof of principle”, but other model building directions should be viable as well. Within the context of the specific constructions presented here, it would be worthwhile to try to flesh out a more detailed structure for the composite dark matter particles, along with a corresponding cosmological history.

Finally, considering form factor dark matter in the context of a possible “channeling” effect [36, 37] in the DAMA/NaI detector seems to be a very promising direction, and will be the subject of a future paper [38].

Note added: After this paper appeared on arXiv, there appeared [39], which considers certain dark matter form factors in the context of spin-dependent cross-sections.

## Acknowledgments

We have benefited from conversations with A. Cohen, D. Finkbeiner, M. McCullough, B. Tweedie, J. Wacker, and N. Weiner. We especially would like to thank M. Kuhlen for comments on uncertainties regarding modeling the dark matter halo. BF is supported by DOE grant DE-FG02-01ER-40676, ALF is supported by DOE grant DE-FG02-01ER-40676 and NSF CAREER grant PHY-0645456, and EK is supported by DOE grant DE-FG02-01ER-40676, NSF CAREER grant PHY-0645456, and an Alfred P. Sloan Fellowship.

## References

- [1] R. Bernabei *et al.* [DAMA Collaboration], “First results from DAMA/LIBRA and the combined results with DAMA/NaI,” *Eur. Phys. J. C* **56**, 333 (2008) [arXiv:0804.2741 [astro-ph]].
- [2] R. Bernabei *et al.* [DAMA Collaboration], “Search for WIMP annual modulation signature: Results from DAMA / NaI-3 and DAMA / NaI-4 and the global combined analysis,” *Phys. Lett. B* **480**, 23 (2000).
- [3] M. Fairbairn and T. Schwetz, “Spin-independent elastic WIMP scattering and the DAMA annual modulation signal,” *JCAP* **0901**, 037 (2009) [arXiv:0808.0704 [hep-ph]].
- [4] D. Tucker-Smith, N. Weiner, “Inelastic Dark Matter,” *Phys. Rev. D* **64**, 043502 (2001) [arXiv:hep-ph/].
- [5] S. Chang, G. D. Kribs, D. Tucker-Smith and N. Weiner, *Phys. Rev. D* **79**, 043513 (2009) [arXiv:0807.2250 [hep-ph]].
- [6] J. March-Russell, C. McCabe and M. McCullough, “Inelastic Dark Matter, Non-Standard Halos and the DAMA/LIBRA Results,” *JHEP* **0905**, 071 (2009) [arXiv:0812.1931 [astro-ph]].
- [7] Y. Cui, D. E. Morrissey, D. Poland and L. Randall, “Candidates for Inelastic Dark Matter,” *JHEP* **0905**, 076 (2009) [arXiv:0901.0557 [hep-ph]].

- [8] D. P. Finkbeiner, T. Lin and N. Weiner, “Inelastic Dark Matter and DAMA/LIBRA: An Experimentum Crucis,” arXiv:0906.0002 [astro-ph.CO].
- [9] K. Schmidt-Hoberg and M. W. Winkler, “Improved Constraints on Inelastic Dark Matter,” arXiv:0907.3940 [astro-ph.CO].
- [10] J. D. Lewin and P. F. Smith, “Review of mathematics, numerical factors, and corrections for dark matter experiments based on elastic nuclear recoil,” *Astropart. Phys.* **6**, 87 (1996).
- [11] P. F. Smith and J. D. Lewin, “Dark Matter Detection,” *Phys. Rept.* **187**, 203 (1990).
- [12] G. Duda, A. Kemper and P. Gondolo, “Model independent form factors for spin independent neutralino nucleon scattering from elastic electron scattering data,” *JCAP* **0704**, 012 (2007) [arXiv:hep-ph/0608035].
- [13] G. Fricke et al., “Nuclear Ground State Charge Radii from Electromagnetic Interactions,” *Atomic Data and Nuclear Data Tables* **60**, 177 (1995).
- [14] M. C. Smith *et al.*, *Mon. Not. Roy. Astron. Soc.* **379**, 755 (2007) [arXiv:astro-ph/0611671].
- [15] J. L. Feng, J. Kumar and L. E. Strigari, “Explaining the DAMA Signal with WIMPless Dark Matter,” *Phys. Lett. B* **670**, 37 (2008) [arXiv:0806.3746 [hep-ph]].
- [16] F. Petriello and K. M. Zurek, “DAMA and WIMP dark matter,” *JHEP* **0809**, 047 (2008) [arXiv:0806.3989 [hep-ph]].
- [17] A. Bottino, F. Donato, N. Fornengo and S. Scopel, “Interpreting the recent results on direct search for dark matter particles in terms of relic neutralino,” *Phys. Rev. D* **78**, 083520 (2008) [arXiv:0806.4099 [hep-ph]].
- [18] R. Foot, “Mirror dark matter and the new DAMA/LIBRA results: A simple explanation for a beautiful experiment,” *Phys. Rev. D* **78**, 043529 (2008) [arXiv:0804.4518 [hep-ph]].
- [19] P. Gondolo and G. Gelmini, “Compatibility of DAMA dark matter detection with other searches,” *Phys. Rev. D* **71**, 123520 (2005) [arXiv:hep-ph/0504010].
- [20] S. Chang, A. Pierce and N. Weiner, “Using the Energy Spectrum at DAMA/LIBRA to Probe Light Dark Matter,” arXiv:0808.0196 [hep-ph].
- [21] S. Yellin, *Phys. Rev. D* **66**, 032005 (2002) [arXiv:physics/0203002].
- [22] J. Diemand, M. Kuhlen and P. Madau, “Dark matter substructure and gamma-ray annihilation in the Milky Way halo,” *Astrophys. J.* **657**, 262 (2007) [arXiv:astro-ph/0611370].

- [23] D. S. Akerib *et al.* [CDMS Collaboration], “First results from the cryogenic dark matter search in the Soudan Underground Lab,” *Phys. Rev. Lett.* **93**, 211301 (2004) [arXiv:astro-ph/0405033].
- [24] D. S. Akerib *et al.* [CDMS Collaboration], “Limits on spin-independent WIMP nucleon interactions from the two-tower run of the Cryogenic Dark Matter Search,” *Phys. Rev. Lett.* **96**, 011302 (2006) [arXiv:astro-ph/0509259].
- [25] Z. Ahmed *et al.* [CDMS Collaboration], “Search for Weakly Interacting Massive Particles with the First Five-Tower Data from the Cryogenic Dark Matter Search at the Soudan Underground Laboratory,” *Phys. Rev. Lett.* **102**, 011301 (2009) [arXiv:0802.3530 [astro-ph]].
- [26] G. Angloher *et al.*, “Limits on WIMP dark matter using scintillating CaWO<sub>4</sub> cryogenic detectors with active background suppression,” *Astropart. Phys.* **23**, 325 (2005) [arXiv:astro-ph/0408006].
- [27] G. Angloher *et al.*, “Commissioning Run of the CRESST-II Dark Matter Search,” arXiv:0809.1829 [astro-ph].
- [28] R. F. Lang and W. Seidel, “Search for Dark Matter with CRESST,” arXiv:0906.3290 [astro-ph.IM].
- [29] J. Angle *et al.* [XENON Collaboration], “First Results from the XENON10 Dark Matter Experiment at the Gran Sasso National Laboratory,” *Phys. Rev. Lett.* **100**, 021303 (2008) [arXiv:0706.0039 [astro-ph]].
- [30] X. Collaboration, “Constraints on inelastic dark matter from XENON10,” arXiv:0910.3698 [astro-ph.CO].
- [31] G. J. Alner *et al.*, “First limits on WIMP nuclear recoil signals in ZEPLIN-II: A two phase xenon detector for dark matter detection,” *Astropart. Phys.* **28**, 287 (2007) [arXiv:astro-ph/0701858].
- [32] V. N. Lebedenko *et al.*, “Result from the First Science Run of the ZEPLIN-III Dark Matter Search Experiment,” arXiv:0812.1150 [astro-ph].
- [33] S. K. Kim [KIMS Collaboration], “New results from the KIMS experiment,” *J. Phys. Conf. Ser.* **120**, 042021 (2008).
- [34] J. D. Bjorken, R. Esseg, P. Schuster, N. Toro, “New Fixed-Target Experiments to Search for Dark Gauge Forces,” [arXiv:0906.0580 [hep-ph]].
- [35] R. Esseg, P. Schuster, N. Toro, “Probing Dark Forces and New Hidden Sectors at Low-Energy e<sup>+</sup>e<sup>-</sup> Colliders,” [arXiv:0903.3941 [hep-ph]].

- [36] E. M. Drobyshevski, “Channeling Effect and Improvement of the Efficiency of Charged Particle Mod. Phys. Lett. A **23**, 3077 (2008) [arXiv:0706.3095 [physics.ins-det]].
- [37] R. Bernabei *et al.*, “Possible implications of the channeling effect in NaI(Tl) crystals,” Eur. Phys. J. C **53**, 205 (2008) [arXiv:0710.0288 [astro-ph]].
- [38] B. Feldstein, A. L. Fitzpatrick, E. Katz and B. Tweedie, “A Simple Explanation for DAMA with Moderate Channeling,” arXiv:0910.0007 [hep-ph]
- [39] S. Chang, A. Pierce and N. Weiner, “Momentum Dependent Dark Matter Scattering,” arXiv:0908.3192 [hep-ph].